Journal of Applied Remote Sensing

RemoteSensing.SPIEDigitalLibrary.org

Reflectance-based skin detection in the short wave infrared band and its application to video

Tye Langston

SPIE.

Tye Langston, "Reflectance-based skin detection in the short wave infrared band and its application to video," *J. Appl. Remote Sens.* **10**(4), 046026 (2016), doi: 10.1117/1.JRS.10.046026.

Reflectance-based skin detection in the short wave infrared band and its application to video

Tye Langston*
Naval Surface Warfare Center, 110 Vernon Avenue, Panama City, Florida 33407, United States

Abstract. Robust reflectance-based skin detection is a potentially powerful tool for security and search and rescue applications, especially when applied to video. However, to be useful it must be able to account for the variations of human skin, as well as other items in the environment that could cause false detections. This effort focused on identifying a robust skin detection scheme that is appropriate for video application. Skin reflectance was modeled to identify unique skin features and compare them to potential false positive materials. Based on these comparisons, specific wavelength bands were selected and different combinations of two and three optical filters were used for actively identifying skin, as well as identifying and removing potential false positive materials. One wavelength combination (1072/1250 nm) was applied to video using both single- and dual-camera configurations based on its still image performance, as well as its appropriateness for video application. There are several important factors regarding the extension of still image skin detection to video, including light available for detection (solar irradiance and reflectance intensity), overall intensity differences between different optical filters, optical component light loss, frame rate, time lag when switching between filters, image coregistration, and camera auto gain behavior.
[DOI: 10.1117/1.JRS.10.046026]

Keywords: skin detection; remote sensing; short wave infrared.

Paper 16297 received Apr. 20, 2016; accepted for publication Nov. 8, 2016; published online Dec. 14, 2016.

1 Introduction

The spectral variation of skin reflectance is potentially useful in several ways. This information can be used to assess the health,[1–7] activity level,[8,9] emotional state,[8,9] and physical characteristics of a person,[5,6,10–13] to tailor specific dermatologic treatments,[7,14–16] or for human detection.[17–22] This effort focuses on the latter; the usefulness of this information as a way to detect human skin, with the ultimate focus on the application to video. Robust skin detection offers potential as a valuable asset for search and rescue efforts, as well as for security applications. There are several existing approaches for identifying a person in a scene, including color-based methods,[23–30] infrared (IR) detection,[19,31] pattern matching,[24,26,29,32] and different hyperspectral methods.[4,5,18,33,34] Each of these is appropriate for some situations but has difficulty in others.

The difficulties in most skin detection methods usually arise from similar items in the environment or from the natural biological diversity of skin reflectance. Thus, this effort focuses on identifying skin features that are consistent across different skin types, as well as different from common items found in typical environmental settings. As a first step, a biophysical skin model is constructed that provides reflectance as a function of wavelength and allows for the manipulation of several skin properties. These skin properties, which affect skin reflectance and naturally vary across human populations, include the amount of blood, oxygen saturation level, collagen concentration, melanin concentration, beta-carotene concentration, bilirubin concentration, and subcutaneous reflectance. For this model, skin is divided into 10 separate layers, starting with the stratum corneum and ending with subcutaneous fat. The stratum lucidum layer was

*Address all correspondence to: Tye Langston, E-mail: tye.langston@navy.mil

1931-3195/2016/$25.00

included in the model, but its thickness was usually set to zero because it only occurs in the palms, fingertips, and soles of the feet.

The skin model used for this effort is based on the earlier work by Nunez,[33] Kubelka et al.,[35–37] Dawson et al.,[38] and Meglinski and Matcher.[39] The Kubelka–Munk model (K–M model) is one of the earliest and most well-known works on this topic. It utilizes the absorption and scattering coefficients of paint layers to determine their spectral reflectance. The K–M model has been applied and modified numerous times since its inception in 1931,[35] including by Meglinski and Matcher, who created a hybrid model with the Fresnel equations to account for reflectance at the air–skin interface, where a high differential in the indices of refraction exists. Nunez extended the work of Meglinski and Matcher by collecting *in vivo* and *ex vivo* optical human skin data and incorporating it into their seven layer model. In addition to Nunez's data, the experimental skin parameter data used in the current model came from several different sources.[14,39–46]

Models based on the K–M theory have some inherent limitations, as most models do. For example, K–M models often consider skin to be of a finite number of constant-thickness layers of homogeneous optical properties, when in reality, layer thicknesses can vary and the optical properties can vary within a layer type (such as at particulate-like distribution of melanosomes). In addition, the K–M theory absorption and scattering coefficients are assumed to be linear functions of the intrinsic material absorption and scattering coefficients, but it is argued by Yang, Kruse, and Miklavcic[47–49] that these coefficient sets share a nonlinear relationship. However, despite its shortcomings, the K–M theory has its place. This effort focuses on achieving a real-time, reliable skin detection method that can be applied to video in the field. As such, the K–M theory is considered to be appropriate. With enough computational power, time, and budget, higher fidelity skin modeling can be accomplished, but it is not always warranted.

This effort's skin model is compared to published experimental data for verification and used to identify specific spectral regions that (1) can potentially be used to remotely identify skin; (2) are consistent across the normal biological variations of skin and; and (3) which appear to be different from possible environmental confusers. Using these selected spectral ranges, sets of two and three optical bandpass filters are applied along with detection algorithms to identify skin in scenes that also contain several items that could be confused with skin.

Finally, the last part of this effort is to extend the skin detection to video. Two different systems are constructed and tested: a dual-camera system and a single-camera system. Each type is found to have its own advantages and disadvantages. The dual-camera system identifies human skin by comparing frames from individual cameras that are filtered differently. Three different single camera designs are presented, all of which utilize some type of filter that changes its spectral properties between alternating frames. Special considerations are also identified for skin detection in video that become more influential when extending still image skin detection to video, such as the importance of the amount of light available for detection (solar irradiance and skin reflectance), frame rate, coregistration of images, differences in gain between differently filtered images, and how to rapidly combine different images that have been filtered at different wavelengths.

2 Skin Model

Human skin is complex with many unique characteristics and optical properties that may be exploited for detection. It has several different chromophoric constituents and is roughly divided into multiple different layers. For this model, 10 different layers were considered, which can be categorized as the epidermis layers, dermis layers, and the subcutaneous fat. The strata layers include the stratum corneum, stratum lucidum, stratum granulosum, stratum spinosum, and stratum basale. Melanocytes, which weigh heavily in the visible spectrum, are found in the stratum basale. Although the stratum lucidum layer was included in the model, its thickness was usually set to zero because it only occurs in the palms, fingertips, and soles of the feet.[50,51] The dermis layers consist of the papillary dermis, upper blood net dermis, reticular dermis, and deep blood net dermis. These layers, their thicknesses, and their organization are described in Fig. 1, as well as their blood and water fractions.

Layer	Thickness	Blood fraction	Water fraction	
Stratum corneum	8–20 μm	0	0.05	Epidermis
Stratum lucidum	0–10 μm	0	0.2	
Stratum granulosum	3–5 μm	0	0.2	
Stratum spinosum	50–150 μm	0	0.2	
Stratum basale	15 μm	0	0.2	
Papillary dermis	150 μm	0.04	0.5	Dermis
Upper blood net dermis	80 μm	0.3	0.6	
Reticular dermis	1500 μm	0.04	0.7	
Deep blood net dermis	100 μm	0.1	0.7	
Subcutaneous fat	6000 μm	0.05	0.7	Subcutaneous fat

Fig. 1 Names, order, and thicknesses of skin layers used in the model, along with blood and water fractions. Skin thicknesses were taken from Anderson and Parrish,[15] Meglinski and Matcher,[39] Fore-Pfliger,[50] Nunez,[33] and Koruga et al.[51] Blood fractions were estimated from Meglinski and Matcher,[39] Chapman,[52] Stenn,[53] Odland,[54] Holdbrook,[55] Renkin et al.,[56] Ryan,[57] and Jacques.[58] Water fractions were estimated from Meglinski and Matcher,[39] Chapman,[52] and Potts.[59]

Of course, the actual anatomy of human skin is not as simple as a perfectly layered material as shown in Fig. 1. The relative thicknesses, as well as the absolute thicknesses, can vary from person to person and between different bodily regions. For example, epidermis on the palms of the hands and soles of the feet is around 40 times thicker than that of the eyelids.[50] And the dermis of the back is much thicker than on the abdomen. As previously mentioned, the stratum lucidum layer only occurs in the palms, fingertips, and soles of the feet. And although skin is roughly layered, the layers are not always that well defined. For example, although higher proportions of blood can be found in the upper blood net dermis and deep blood net dermis, it can also be found in lower quantities in the papillary dermis, reticular dermis, and subcutaneous fat.[39] The optical properties of blood also vary with its oxygenation state. Oxygenated hemoglobin absorption peaks at around 415 nm, while unoxygenated hemoglobin absorption peaks at around 433 nm.[60] And the concentration of hemoglobin in the blood also varies from person to person, as well as between veins and arteries. Thus, considering all of these complexities, several assumptions (as described by Nunez[33]) were necessary in the model: (1) a typical skin thickness is considered; (2) skin consists of a finite number of layers; (3) each layer has a constant thickness; (4) each layer has homogeneous optical properties throughout and the properties change instantaneously at the interfaces; and (5) normal incidence is assumed and the upper surface of skin is assumed to be a Lambertian surface with a specular component.

Each layer is somewhat different from its adjacent layers, not only in thickness, but also in composition and optical properties. It may contain different proportions of blood, oxygenated hemoglobin, deoxygenated hemoglobin, collagen, melanin, lipid, beta-carotene, and bilirubin, and each of these constituents possesses unique optical characteristics. Table 1 lists some of the variables within the skin model that could be specifically tailored between runs, as well as their ranges considered in the model. The proportion of collagen for each layer was considered to be the remainder after the blood, water, and melanosome fractions were accounted for. This provides reasonable agreement with the literature.[61–63]

For this effort, the importance of all of the properties listed in Table 1 is in how they affect skin's optical properties, which, of course, varies with wavelength. To allow the model to provide spectrally unique results, wavelength-dependent absorption coefficients for all of these properties were provided to the model. This data were obtained from various sources, including Du et al.[40] (beta-carotene and bilirubin), Prahl[41] (hemoglobin), Pope and Fry[42] and Palmer and Williams[43] (water), van Veen et al.[44] and Altshuler et al.[14] (lipid), Nunez[33] (collagen), and Sarna and Swartz[45] and Thody et al.[46] (melanin). The subcutaneous reflectance data were from cadaver measurements by Nunez.[33]

The skin model created for this effort is based on the earlier work by Nunez,[33] Kubelka et al.,[35–37] Dawson et al.,[38] Meglinski and Matcher,[39] and Jacques.[63] The K–M model is one

Table 1 Skin composition property values used in the model.

Skin property	Value
Melanosome fraction (stratum spinosum and stratum basale)	0.016 to 0.43[64,63]
Beta-carotene concentration in blood	$7(10^{-5})$ g/L[65]
Beta-carotene concentration in epidermis	0.21 to 0.9 μg/g[65]
Beta-carotene concentration in dermis	0.07 μg/g[65]
Hemoglobin concentration in blood	134 to 173 g/L[1,66]
Bilirubin concentration in blood	0.009 to 0.22 g/L[67]
Hemoglobin oxygenation fraction	0.93 to 0.99 (arteries), 0.40 to 0.80 (veins)[30,68,69,70,71,72]
Reflectance of subcutaneous fat	0.45 to 0.7[33]

of the earliest and most well-known works on this topic and it has been applied numerous times since its inception in 1931.[35] Dawson et al. further developed the theory for light transmission and reflection in layered materials, while Meglinski et al. extended the K–M model to account for reflectance at the air–skin interface. Nunez collected *in vivo* and *ex vivo* optical human skin data, which are applicable to some of the individual skin layers considered in K–M models. The methodology for the skin detection model can be described in four steps.

Step 1: Model the Fresnel reflection at the air/skin (stratum corneum) interface. The Fresnel equation, as discussed by Hecht,[73] takes into account the indices of refraction of the two interfacing materials to determine the reflection. It is only valid at normal incidence and can be computed as

$$F = \left(\frac{\eta_2 - \eta_1}{\eta_2 + \eta_1}\right)^2, \tag{1}$$

where η_1 is the index of refraction for air and η_2 is the index of refraction for the uppermost skin layer, the stratum corneum.

Step 2: Determine the transmission and reflection of each individual layer. Kubelka and Munk[35–38] have provided equations that allow for the determination of the transmission and reflection of homogeneous layers of material with constant optical properties. Each skin layer has unique optical properties, and these equations consider the different scattering and absorption coefficients of the various constituents within each layer as a function of wavelength. The transmission and reflection of the n'th layer as a function of wavelength can be described as

$$t_n(\lambda) = \frac{4\beta_n(\lambda)}{[1+\beta_n(\lambda)]^2 e^{K_n(\lambda)d_n} - [1-\beta_n(\lambda)]^2 e^{-K_n(\lambda)d_n}}, \tag{2}$$

$$r_n(\lambda) = \frac{[1-\beta_n(\lambda)^2](e^{K_n(\lambda)d_n} - e^{-K_n(\lambda)d_n})}{[1+\beta_n(\lambda)]^2 e^{K_n(\lambda)d_n} - [1-\beta_n(\lambda)]^2 e^{-K_n(\lambda)d_n}}, \tag{3}$$

where d_n is the thickness of the n'th layer. The parameters $\beta_n(\lambda)$ and $K_n(\lambda)$ are dependent on the wavelength, λ, and are related to each layer's absorption and scattering properties

$$\beta_n(\lambda) = \sqrt{A_n(\lambda)/[A_n(\lambda) + 2S'_n(\lambda)]}, \tag{4}$$

$$K_n(\lambda) = \sqrt{A_n(\lambda)[A_n(\lambda) + 2S'_n(\lambda)]}, \tag{5}$$

where A_n and S'_n are the absorption and scattering coefficients as a function of wavelength, respectively

$$A_n(\lambda) = \frac{a_{n(\lambda)}}{\frac{1}{2} + \frac{1}{4}\left\{1 - \frac{s'_n(\lambda)}{[s'_n(\lambda)+a_n(\lambda)]}\right\}}, \tag{6}$$

$$S'_n(\lambda) = \frac{s_{n(\lambda)}}{\frac{4}{3} + \frac{38}{45}\left\{1 - \frac{s_n(\lambda)}{[s_n(\lambda)+a_n(\lambda)]}\right\}}. \tag{7}$$

The general scattering coefficient, which depends highly on the collagen content, was based on the equation put forth by Jacques:[63]

$$s = 2(10^{12})\lambda^{-4} + 2(10^{5})\lambda^{-1.5}. \tag{8}$$

Step 3: Sum all of the reflectance and transmittance paths in the first layer. Equations (2) and (3) allow for the determination of the first transmission or reflection path of a single layer. However, each time light encounters an interface, it is partially reflected and partially transmitted, as shown in Fig. 2. This continues until the amount of light remaining in the layer is negligible. Equations (9) and (10) are based on work by Kubelka,[36] Gurevic,[74] and Zocher.[75] They account for an infinite number of diminishing reflections between the air and the first skin layer interface

$$R_1 = r_o + t_o^2 r_1 \sum_{m=0}^{\infty} (r_o r_1)^m, \tag{9}$$

where R_1 is the total reflectance from the first layer, r_o is the reflectance at the air–skin interface (interface 0), r_1 is the reflectance at interface 1, and t_o is the transmittance at the air–skin interface

$$T_1 = t_o t_1 \sum_{m=0}^{\infty} (r_o r_1)^m, \tag{10}$$

where T_1 is the total transmittance through the first layer and t_1 is the transmittance at interface 1.

Step 4: Finally, using the reflectance and transmittance of the first layer, proceed to calculate the total reflectance and transmittance of all layers combined through an iterative process, as shown in Eqs. (11) and (12), which are a continuation of Eq. (9) and (10) above. n represents the interface number

$$R_{n+1} = R_n + T_n^2 r_{n+1} \sum_{m=0}^{\infty} (R_n r_{n+1})^m, \tag{11}$$

$$T_{n+1} = T_n t_{n+1} \sum_{m=0}^{\infty} (R_n r_{n+1})^m. \tag{12}$$

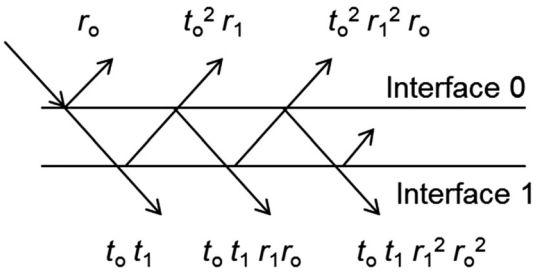

Fig. 2 Illustration of the calculation of skin transmittance and reflectance for the first layer. r_n and t_n represent reflectances and transmittances, respectively. The subscript, n, represents the interface number.

3 Skin Model Output

As previously mentioned, the skin model includes several parameters that may be varied, including subcutaneous reflectance, melanosome fraction, beta-carotene concentration in blood, beta-carotene concentration in the epidermis and dermis, bilirubin concentration in blood, hemoglobin concentration in blood, oxygen saturation, and blood fraction (average concentration of blood in the dermis). Each of these parameters has natural ranges associated with them, with variability coming from person to person differences, physiological state, and ethnicity.

Of all these variables, melanin was by far the most influential on the skin reflectance results. Beta-carotene, bilirubin, and hemoglobin concentration variations all had minimal effect in comparison. Overall blood fraction in the skin and the subcutaneous reflectance also had significant impact but not as much as melanin. Figure 3 shows the changes in reflectance observed when varying the melanosome content, blood fraction, and subcutaneous reflectance from their minimum to maximum values, with all other variables being set to their median values.

The trends shown in Figs. 3(a) and 3(b) are similar to those described by Petrov et al.,[76] who evaluated human skin through *in vivo* transmission measurements and Monte Carlo simulations. They simulated the effect of varying the melanin content (0% to 45%) and blood concentration in the layers from papillary dermis to subcutaneous tissue (0% to 70%) on reflectance from 350 to 1000 nm. They showed a very strong influence from melanin throughout their range that was very similar to Fig. 3(a). Their results also demonstrated a more subtle influence of blood concentration on reflectance in this spectrum, similar to Fig. 3(b), except they indicated a stronger response between 500 and 600 nm for their input parameters.

Upon closer inspection of Fig. 3(a), it can be seen that the influence of melanin on reflectance occurs mostly in the visible region. This is the primary reason why this effort avoided the visible spectrum and instead focused on the short wave infrared (SWIR) region, where the effect of melanin on skin reflectance is much less severe. If we were to focus on the visible region, differences in melanosome content (skin color) would drastically impact the ability to detect skin. Figure 3(a) shows that even the hemoglobin "w" feature between 500 and 600 nm, which is sometimes used for skin evaluation and detection,[2,8,10,30,77] is almost completely washed out with dark skin color. Human skin reflectance has very significant variability in the visible region due to melanin. Considering this large variation in detection will only require a larger variation in the indices that must be considered. Though it is not impossible to detect skin when considering visible reflectance, it was considered prudent in this application to avoid regions where there can be a lot of variation between different individuals. Other researchers have taken a different approach by considering the visible region. For example, Chen et al.[78] focused on modeling the effects of melanin more accurately, while Baranoski et al.[34] proposed a four-wavelength detection index that includes wavelengths from both the visible and near-IR regions. Such an index may perform well but may also be difficult to apply in a video detection system. It would require sensors that cover a large spectral range and the ability to capture and compare four different images per video frame.

To bound the skin reflectance ranges from the model, the variables were combined in a way to achieve the most extreme cases. This is shown in Figs. 4(a) and 5(a), alongside experimental reflectance data from Vyas et al.,[5] Cooksey et al.,[79] Jacquez et al.[80,81] as comparisons in

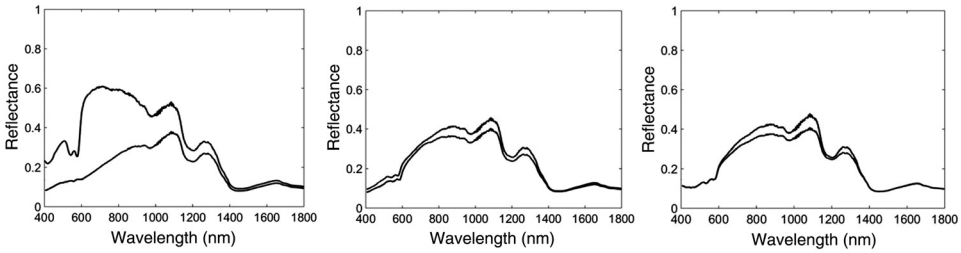

Fig. 3 The effect of varying (a) melanosome fraction, (b) blood fraction, and (c) subcutaneous reflectance from their minimum to maximum values (with all other variables set at their median values).

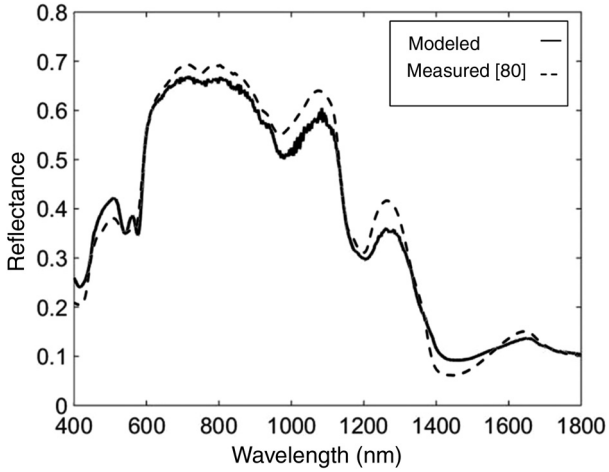

Fig. 4 Maximum reflectance as predicted by the model and as measured by Cooksey et al.[79]

Figs. 4(b) and 5(b), respectively. The data from Cooksey et al.[82] were selected as a comparison for lightly pigmented skin because review of the photographic images of their subjects' skin indicated that they had considered several subjects with visually light skin. However, Cooksey's data were not used as an experimental reference for darkly pigmented skin. None of the available images shown in Ref. 82 showed that they had included subjects with high melanin content. They also indicated that their subjects were not selected based on ethnicity as might be related to skin tone.[79,82] And finally, their lowest reflectance curves exhibited a higher reflectance than that described by Vyas et al., Jacquez et al., and Parra for African American and African skin, respectively. Therefore, for skin with high melanin content, Vyas's and Jacquez's data were considered more appropriate for comparison to the model.[5]

It can be seen that the model output provides reasonable agreement with Cooksey's experimental data on the high end of the range (lightly pigmented), both in magnitude and shape of the reflectance curve. There are some areas where the magnitude differs between the experimental data and the model predictions. These discrepancies may result from slight differences in the actual versus modeled skin properties, inaccuracies in the model, or factors related to the experimental measuring techniques and equipment used.

The model also provides reasonable agreement with the reflectance curves for skin with high melanin content. However, the model also has some differences from both experimental curves. The model is in good agreement with the overall magnitude of reflectance of Vyas's

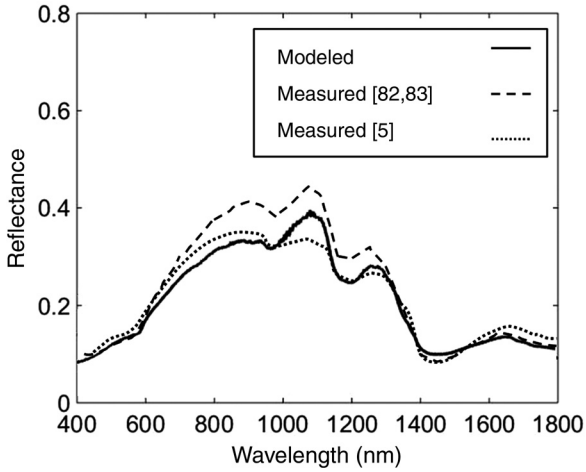

Fig. 5 Minimum (high melanin content) reflectance from model compared to measured reflectance from African American skin as measured by Vyas et al.[5] and Jacquez et al.[80,81]

experimental data, but there is a noticeable difference in the shape of the curve. Specifically, the peak around 1100 nm is more muted in Vyas's data. It was also observed that this peak was also diminished in Vyas's data for lighter skin (Caucasian and Asian) when compared to that of Cooksey et al. As another reference point, Jacquez et al. also measured the reflectance of high melanin content skin. Their curve is more representative of the model in its shape but it shows a somewhat higher reflectance between 700 and 1300 nm. The variations between the different reflectance measurements may be due to differences in measurement technique, equipment, or test subjects.

In the case of a curved shape, the model output is more representative of Cooksey's and Jacquez's data. It is suspected that if Cooksey's data had included skin with high melanin content, there would be a better match in curve shape in this pigmentation range. It can also be noted that Parra[12] studied skin reflectance based on populations with different levels of pigmentation. Although they only reported for a spectral range of 400 to 700 nm, their measured reflectance for skin from African subjects was also on the order of that shown for the model in Fig. 5. These two curves produced by the model (maximum and minimum reflectance) represent the range of reflectances that can be identified as skin.

4 Skin Detection in Still Images

The primary purpose of the skin model was to identify appropriate wavelengths to search for skin, while also avoiding other materials that could create false positives. Figure 6 shows typical skin model output, overlaid with the reflectance profiles of several items that could potentially create false positives, based on either their color or water content, which is heavily influential in the SWIR region. The wavelengths that were chosen for investigations are also marked with vertical lines.

It can be seen that there are some similarities and differences between the reflectance of skin and the potential confusers shown in Fig. 6. As previously mentioned, skin detection was avoided in the visible and near-IR regions because of the high variability of skin reflectance with melanosome concentration. Focusing instead in the SWIR range, a few different features are noticed with skin reflectance. There is a strong reflectance peak around 1100 nm, as well as a subsequent one at around 1250 nm. There is also a dip around 1450 nm and another small peak around 1650 nm. The purpose herein was not just to identify unique characteristics of skin for detection but also to identify characteristics that were different from other potential confusers. Each of these spectral features was considered for skin detection, and particular wavelengths were chosen based on the practical availability of optical bandpass filters.

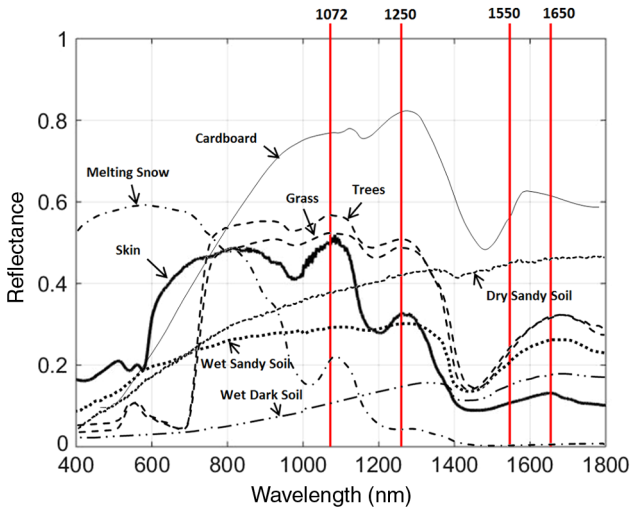

Fig. 6 Reflectance of skin and some potential confusers (grass,[83] trees,[83] cardboard,[83] dry sandy soil,[83,84] wet sandy soil,[84] wet dark soil,[84] and melting snow.[85] Also shown are wavelengths of interest that represent unique skin features and available optical bandpass filter designations.

1072 nm: There is a strong peak for skin reflectance at this wavelength. The high level of reflectance means that a reflectance signature should be available for measurement even in lower light conditions. Because of this strong peak and the relative consistency across different skin types, 1072 nm was chosen as the primary (reference) wavelength for skin detection efforts.

1250 nm: There is also a fairly strong reflectance for skin at this wavelength and when comparing the 1072-/1250-nm ratio between skin and the other materials in Fig. 6, there is a significant difference. For cardboard and soil (wet or dry), the reflectance is higher at 1250 than at 1072, opposite that of skin. And for vegetation (grass and trees), the 1250-nm reflectance is much closer to the 1072 reflectance than that of skin.

1450 nm: The region around 1450 nm also exhibits a unique reflectance feature that is worth discussing. A strong dip occurred here that was most prominent with skin and vegetation. This is due to the strong absorption peak of water in this range. This region was avoided because the strong absorption means that very little overall reflectance would be expected for skin, making it difficult to measure, especially in low light conditions. This is also compounded by the fact that atmospheric absorption of light in this range is very strong due to the presence of water in the atmosphere. Very little solar illumination at 1450 nm even reaches the subject in natural lighting conditions. Both of these factors mean that very little signal is available to detect. Figure 7 provides a plot of solar spectral irradiance from Ref. 86.

1550 nm: Skin's reflectance at 1550 nm is much lower than that of the other materials shown in Figure 6. Because a significant difference in the 1072-/1550-nm ratio can be achieved between skin and the other materials, this wavelength was considered. This combination is also very similar to that used by Nunez[33] (1080/1580 nm), with which he reported good results. Furthermore, the atmosphere has lower absorption at 1550 nm than it does at 1450 nm, allowing more radiation to reach the earth's surface. A drawback to this wavelength is that although reflectance is greater than that at 1450 nm, skin still has a generally low reflectance here, potentially making detection difficult in low light conditions. Furthermore, it has also been reported that skin has similar reflectance to some water and soil mixtures between 1450 and 1650 nm.[34]

1650 nm: The reflectance of skin at this wavelength is slightly higher in magnitude than that at 1550 nm, and the 1072-/1650-nm reflectance ratio is much different for skin versus the other materials. Therefore, this wavelength was also considered.

For skin detection measurements, identical images were captured using each of the bandpass filters, and then compared pixel by pixel to identify which pixels represented the expected reflectance properties of skin. The differences between the two images were processed using a normalized difference index, similar to the normalized difference vegetation index (NDVI)[18] and the normalized difference skin index (NDSI).[33] Considering that 1072 nm was used as the primary reference wavelength, the normalized difference index for this work can be expressed as

$$\mathrm{NI}_i = \frac{\hat{\rho}_i(1072\ \mathrm{nm}) - \hat{\rho}_i(x\ \mathrm{nm})}{\hat{\rho}_i(1072\ \mathrm{nm}) + \hat{\rho}_i(x\ \mathrm{nm})}, \tag{13}$$

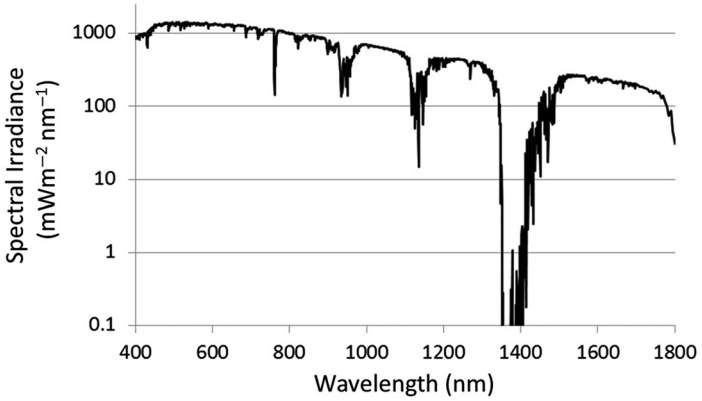

Fig. 7 Solar spectral irradiance (direct + circumsolar).[86]

where NI_i is the normalized index for the i'th pixel and $\hat{\rho}_i$ is the estimated reflectance for the i'th pixel at the indicated wavelength. x represents either 1250, 1550, or 1650 nm.

Because the normalized index is based on reflectance and the different bandpass filters lead to differences in overall image intensity, images must first be converted from radiance to reflectance. One method to accomplish this is to measure the solar irradiance and divide the spectra by it. Another method, the empirical line method (ELM) (described in Ref. 87, makes use of linear regression utilizing in-scene targets with known reflectances. It has been proven and applied with success by previous researchers[33,87] For convenience, the ELM was used.

Detection was evaluated both indoors using tungsten-halogen lamps and outdoors under natural illumination. Tungsten-halogen lamps were used indoors because they provide broad spectrum illumination, as well as a good representation of the illumination from the sun within the spectral ranges considered. Most other indoor lighting types, such as incandescent, fluorescent, compact fluorescent, and light-emitting diode are confined mostly to the visible range and are often comprised of lighting from only a few different distinct bands.

Figure 8 provides a photograph of an indoor scene used for skin detection analysis. It can be seen that along with subjects of different skin tones, several potential confusers were also included in the scene to challenge the method, such as vegetation, cardboard, leather, a skin-tone brick, dry sand, wet sand, and a human form (dummy). Figure 9 shows the skin detection results for the different two-filter combinations (1072/1250 nm), (1072/1550 nm), and (1072/1650 nm).

For a two-filter system, the 1072-/1250-nm combination performed the best. It was the only one that successfully identified the shadowed skin on the foot of the subject on the left. It also had less trouble with false positives. The 1072-/1550-nm and 1072-/1650-nm combinations both had significant difficulty with the vegetation in the scene, and the 1072/1650 combination seemed to struggle with shadows under the table as well. All of the combinations successfully excluded all of the other potential false positives in the scene (leather, cardboard, wet sand, dry sand, skin-tone brick, and human form). Figure 10 shows in-scene results for the 1072-/1250-nm combination, both inside under tungsten-halogen lighting and outside under ambient light. The outside scene has significant vegetation in the background (grass and trees), as well as sea water, shadows, and several man-made materials. The applicable range of the normalized index depends on the maximum and minimum skin reflectances at the two wavelengths being considered.

For the 1072-/1250-nm combination, the index ranges from 0.19 to 0.24 for modeled reflectance. When considering experimental reflectance data from Cooksey et al. and Jacquez et al.,

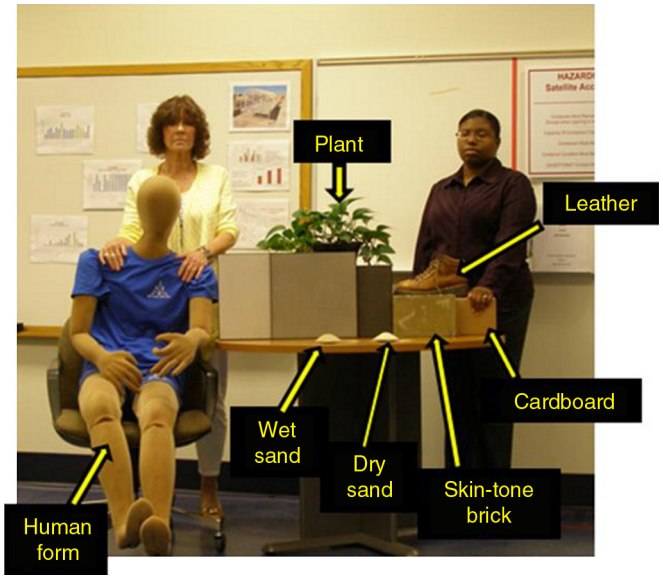

Fig. 8 Photograph of scene with different skin tones and potential confusers (vegetation, leather, cardboard, skin-tone brick, dry sand, wet sand, and human form).

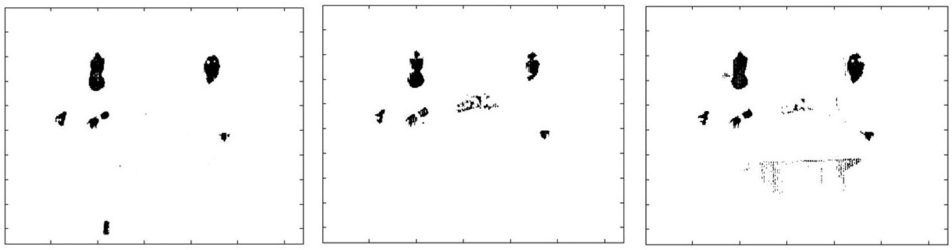

(a) (b) (c)

Fig. 9 Skin detection results for (a) the 1072-/1250-nm filter combination, (b) the 1072-/1550-nm filter combination, and (c) the 1072-/1650-nm filter combination.

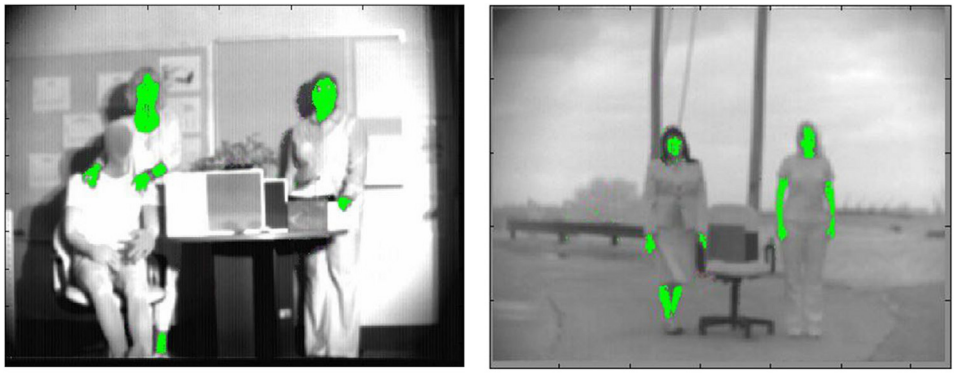

(a) (b)

Fig. 10 Inside and outside skin detection results with the 1072-/1250-nm filter combination.

the index ranges from 0.18 to 0.23. As a comparison, the NDSI range for the 1080-/1580-nm wavelength pair by Nunez[33] is reported as 0.66 to 0.77 and the MDSI range for the 450/650/1450/1650 wavelength set by Baranoski and Chen[34] is reported as 0.16 to 0.18. As an additional comparison, Table 2 shows the 1072/1250 index values for several other materials, along with that of modeled and measured skin reflectance. Although there are countless materials and material combinations in nature, Table 2 shows that the 1072-/1250-nm pair results in an index that leaves a broad range of materials well outside the index range of skin.

Table 2 Comparison of 1072-/1250-nm pair index for skin and other materials.

Material	1072/1250 NI index value
Skin (modeled)	0.19 to 0.24
Skin (reflectance data)[79–81]	0.18 to 0.23
Cardboard[83]	−0.09
Trees[83]	0.05
Grass[83]	0.03
Dry sandy soil[83,84]	−0.05
Wet sandy soil[84]	−0.02
Wet dark soil[84]	−0.15
Melting snow[85]	0.66

5 Three-Filter Skin Detection for Active Rejection of False Positives

The reflectance of skin in the SWIR region is much more stable than in the visible spectrum due to the reduced influence of melanin. However, skin reflectance in this range can be similar to other materials, such as vegetation and in some cases, shadows. Vegetation, such as skin, contains a significant amount of water, which plays an important role in the SWIR band. To address this, an effort was made to use a third filter to help with false positive rejection in the filter combinations that had trouble with vegetation. The idea was to actively identify vegetation and then subtract it from the image. In previous works, vegetation has been identified with the NDVI using 860- and 660-nm wavelengths.[88,89] However, because we focused on a different spectral region and wanted to minimize the number of filters, vegetation was identified using a different wavelength set. As can be seen in Fig. 6, the reflectance of vegetation is similar to skin at 1072 nm. However, it is significantly higher than skin at 1250 and 1650 nm. This offers an opportunity to selectively identify vegetation and remove it from the skin detection results. The 1072 nm was once again used as a reference wavelength. Using the third filter, any ratios that matched vegetation were identified and then those pixels were subtracted from the skin detection results. Figures 11 and 12 show the skin detection results with and without the active subtraction of vegetation.

By applying the third filter approach, the results were clearly improved for the 1072-/1550-nm wavelength set, bringing its performance to that achieved with the 1072-/1250-nm set. The detection of both the vegetation and shadows under the table was reduced. But even though use of the third filter resulted in an improvement, practicality must also be considered. The three-filter

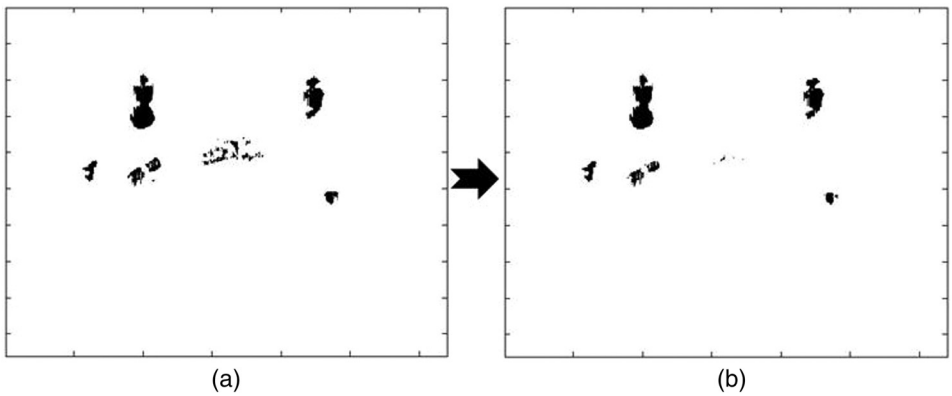

Fig. 11 Skin detection results with and without subtraction of vegetation. (a) The two-filter method (1072/1550 nm) and (b) the three-filter method [1072/1550 nm (skin) and 1072/1250 nm (vegetation)].

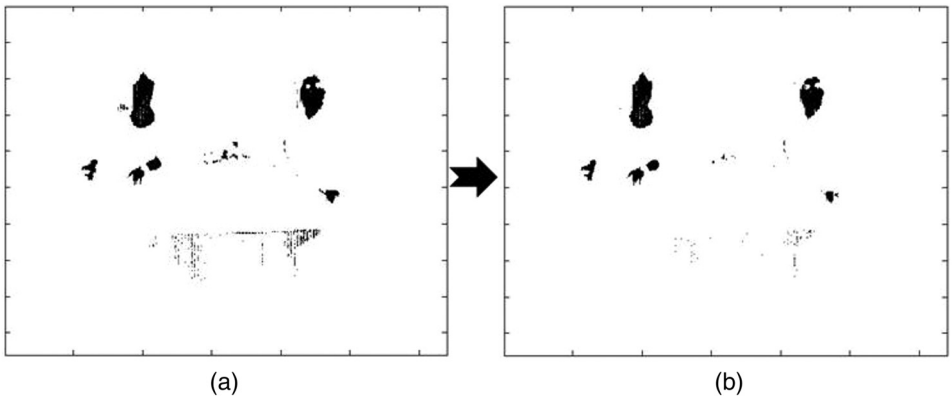

Fig. 12 Skin detection results with and without subtraction of vegetation. (a) The two-filter method (1072/1650 nm) and (b) the three-filter method [1072/1550 nm (skin) and 1072/1250 nm (vegetation)].

method is a more complicated and slower process and a designer has to decide if the improved detection accuracy is worth these drawbacks, especially when applying the system to a video, which needs to be rapid and require minimal computation. In addition, the third filter approach specifically targeted the material that presented the most challenge: vegetation. It may not apply to other materials that could lead to false detections. The best two-filter index (1072/1250 nm) also provided good detection with minimal false detection problems and was much more practical. Thus, the 1072-/1250-nm set was chosen for application to video.

6 Skin Detection in Video

Because the skin detection premise requires the comparison of at least two different images, acquired through different bandpass filters, the application to video requires filtering individual video frames differently and then comparing them. There are two different ways to accomplish this: a single-camera system that is filtered differently for alternating frames, or a multicamera system, where each camera is affixed with a different filter. Each approach has advantages and disadvantages. For this work, only a two-filter combination was considered in the application to video. This is because although the 1072-/1550-/1250-nm three-filter system improved the performance to some degree, the 1072-/1250-nm filter combination also proved adequate and leaving out the third filter reduced complexity. And as will be explained more below, the 1072-/1250-nm filter combination was also found favorable for video application because the reflectances at these two wavelengths were large and somewhat close in magnitude.

One of the major challenges with either the single- or dual-camera approach is acquiring differently filtered images rapidly and computing the skin detection results fast enough to keep up with the desired video frame rate. For a dual-camera system, changing the filter is not required because each camera is permanently fitted with a specific filter, but with a single-camera system, the filtration wavelength must be changed between alternating frames. Another challenge for both types is associated with the camera gain. The reflectance of skin and the environment in general varies with wavelength. When different filters are applied, differences in the overall intensity of the resulting image will also vary. Normally, camera auto-gain correction can easily account for intensity changes. However, in the case of skin detection, differences in intensity between the filtered images are problematic, requiring the detection algorithm to account for the intensity variations by either measuring and dividing by the ambient illumination, or making use of materials in the scene with known reflectances. Known materials are not always available and comparing to ambient illumination can be problematic when it varies across the scene (such as in shadows).

The gain problem is further complicated when utilizing a single-camera system. Cameras with auto-gain control usually average several frames before changing gain. But in a situation like this, gain would need to change for every alternating frame, making for erratic, rapid gain changing operation. Furthermore, for the camera to set a gain value for the upcoming frame, it must have some prior knowledge of the scene illumination, and it would be required to only consider prior frames that were taken under the applicable filter.

The sensitivity to gain of both single- and dual-camera systems is another reason why the 1072-/1250-nm filter combination is more attractive than the 1072/1550 or 1072/1650 combinations for video; the reflectance magnitude at these wavelengths has a smaller differential than the other pairs, meaning that less gain change is required between image pairs. Furthermore, a single gain setting can often be used to cover both filter wavelength intensities, mostly eliminating problems with intensity differences between alternating filter images. Additionally, another benefit of these two wavelengths, versus the others considered, is that the overall magnitude of solar irradiance and skin reflectance is greater for both of them than the others considered, providing greater signature in low light conditions.

6.1 *Dual-Camera System*

A dual-camera system allows for two different video streams to be captured separately and then compared and analyzed for skin presence. As shown in Fig. 13, each camera is fitted

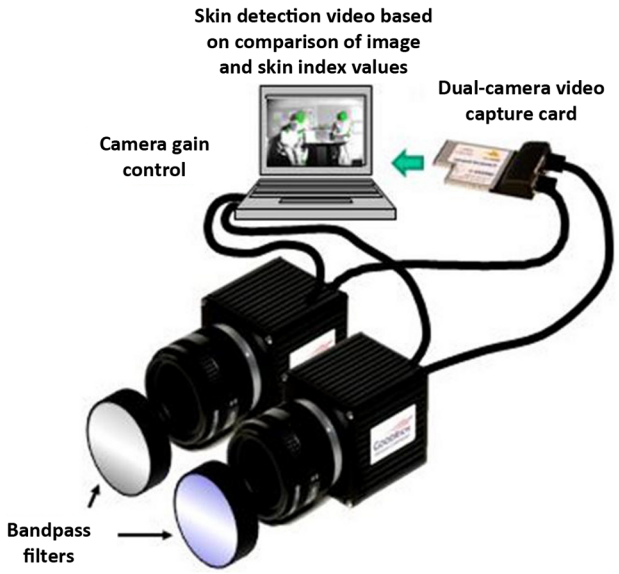

Fig. 13 Dual-camera skin detection video approach.

with a different optical bandpass filter and then images from both cameras are processed together.

The dual-camera approach was the simplest to implement in the laboratory and has some advantages, as well as disadvantages when compared to a single-camera system.

Advantages

- Low light loss due to the minimal number of optical components in front of each camera (one filter only). This leads to better performance in low light conditions.
- A high skin detection video frame rate can be produced, because each video frame can be used to create a skin detection image. In a dual-camera system, the skin detection video can be the same frame rate as the original video. However, in a single-camera system, the frame rate is halved or slower because alternating frames are filtered differently and then compared.

Disadvantages

- Two cameras are required, which are expensive and demand more power.
- Two different gains are in play. Either this must be accounted for by measuring and considering the ambient illumination or in-scene objects of known reflectance, or both gains must be synchronized. For gain synchronization, either both gains must be fixed or if an automatic gain control is used, one camera must be slaved to the other.
- Dual images must be coregistered due to the difference in physical position of the individual camera lenses. And because of the differences in perspective, the images may not always match, especially at short viewing distances. This also makes zooming to different depths of field difficult.

The dual-camera system was configured and tested. Figure 14 provides a screenshot from a dual-camera system video, this time with the skin-colored red. The dual-camera system using the 1072-/1250-nm filter combination was found to perform well.

6.2 *Single-Camera System*

A single-camera system is more attractive from a practical standpoint, primarily because only one camera is needed. In addition to eliminating the additional camera, this allows for only one camera gain to be used, eliminating disparities between camera gains that could affect skin detection. However, there are also challenges associated with this approach. The benefits and drawbacks of a single-camera skin detection system are as follows.

(a) (b)

Fig. 14 Screen shot from video of dual-camera skin detection system (a) without skin detection applied and (b) with skin detection.

Advantages

- Only one camera is needed.
- The gain can be automatically matched for both images because it is operated by only one camera. Even when the gain is changed, there is minimal influence. This is because typical cameras sample and adjust their gains much more slowly than the frame rate. Several frames are gathered before the gain adjusts.
- Both images are perfectly coregistered because they are being captured from the same camera.
- Ability to zoom to different depths of field.

Disadvantages

- Requires special optical components to switch back and forth between the two different filter wavelengths.
- The optical configuration is more complex and requires additional components (such as polarizers), which lead to significant light loss.
- Slower skin detection video frame rate. Because at least two frames are required to create a skin detection image, the frame rate is cut in half, or is slower, compared to the original video.

In an effort to create a system that only required one camera, three different setups were conceived. They all utilized a multiplexing technique that used alternating camera frames to create the skin detection images. This is described in Fig. 15. In this figure, frames 1, 3, and 5 represent images taken using one of the two optical filters, and frames 2, 4, and 6 represent images taken using the other one. These odd and even images are then paired and processed through the skin detection algorithm to create skin truth images, which are then recombined into a video format.

This process requires precise synchronization. The device that switches between the two filter wavelengths must provide a trigger to tell the camera when to capture a frame (or trigger a frame grabber to capture a frame from the camera). Figure 16 shows the three different optical configurations and ranks them in order of cost and expected performance. As is typical, cost was directly proportional to expected performance.

Option 1 was considered to be the simplest and highest performance by far, but required a single filter that was designed to pass narrow spectral bands for both of the necessary wavelengths (1072 and 1250 nm). This feature required custom fabrication and made this option prohibitively expensive for this effort. Behind the dual bandpass filter would be a device designed to alternate between the two wavelength bands, consisting of two polarizers and a liquid crystal (LC) switch. The LC switch, using an electrical signal, would vary its retardance so that only one of the wavelengths was properly polarized to pass through the subsequent polarizer. This composite device is referred to as a "wavelength switch."

Option 2 would use two separate filters, but put one of the wavelength switch polarizers (the rear one) to dual use. In this case, it would be split into two separate components, each of which

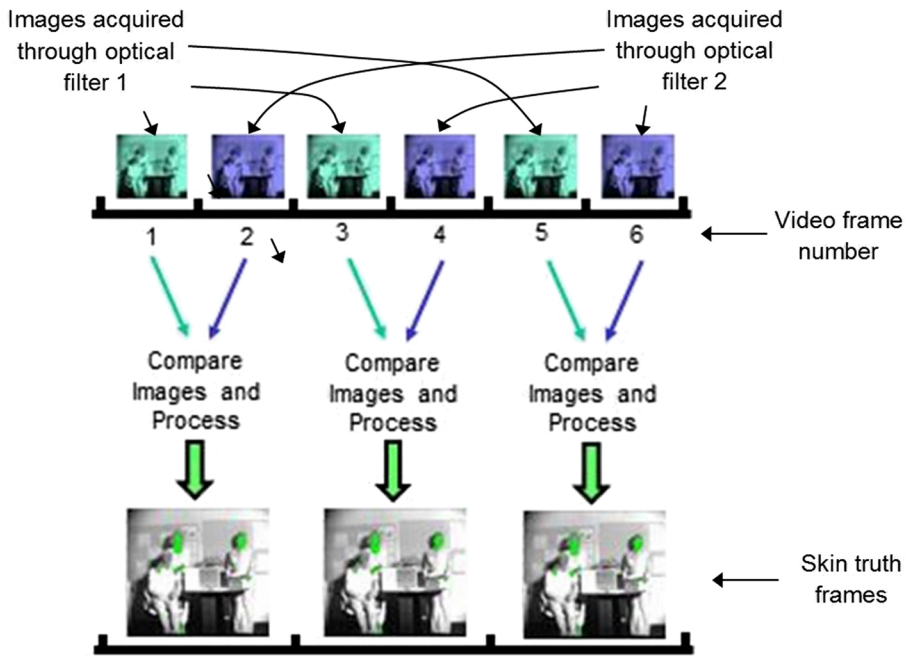

Fig. 15 Multiplexing approach used with single-camera system.

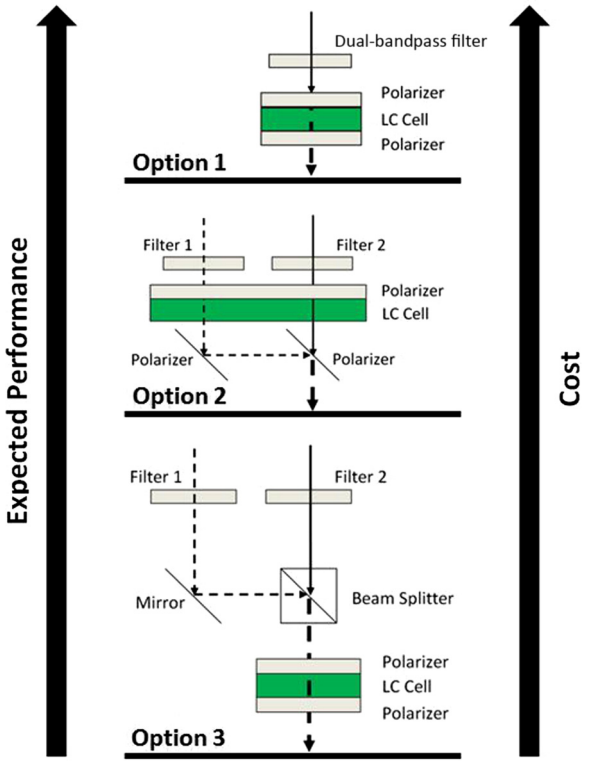

Fig. 16 Options considered for the custom "wavelength switch" to alternate between 1072 and 1250 nm.

would function both as a polarizer and as a reflector, depending on the state of the LC switch. For example, when transmission from filter 1 was desired, the LC switch would change the polarization so that all of the light from both filters was presented to the rear, angled polarizers as S-polarized, which would then reflect off of the polarizers. This meant that the light from filter 2 would be reflected off to the right, while the light from filter 1 would be reflected off of both

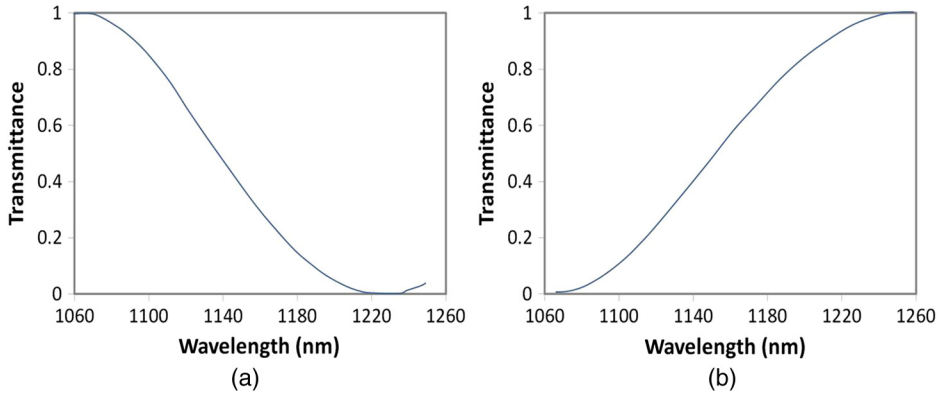

Fig. 17 Custom wavelength switch performance for switched to pass (a) 1072 and (b) 1250 nm.

polarizers, ultimately directing it into the camera. When transmission from filer 2 was desired for the camera, the LC switch altered the polarization of the light coming from both filters, so that it passed through both rear, angled polarizers as P-polarized. This meant that light from filter 1 would pass straight through the left polarizer and go nowhere. The light from filter 2 would pass through the right polarizer and into the camera.

Option 3 was the most complicated and least efficient, but it was also the lowest cost, which is why this option was chosen to demonstrate the concept. Option 3 uses a "wavelength switch" similar to option 1, except it uses two separate bandpass filters. To direct the light passing through both bandpass filters into the wavelength switch, an additional mirror and beam splitter were used.

Figure 17 shows the performance of the custom-made wavelength switch used. It is capable of switching between nearly full passage of one wavelength, while blocking the other, and vice versa. However, it does not have a sharp cutoff for the two wavelengths like Option 1 would. For this reason, the additional bandpass blocking filters are still required in front of the wavelength switch, to reduce the incoming light to only include the 1072 and 1250 bands. Utilizing stereo lithography and three-dimensional printing, an enclosure was fabricated to house and arrange the option 3 optical components.

Figure 18 provides a screenshot of the video obtained with the option 3 configuration while it was alternating between the 1072- and 1250-nm filters in sync with the camera frames. At least one frame was skipped between captures to allow for wavelength-switching time. Using this configuration to capture images for skin detection allowed for the use of only one camera. Skin was successfully identified with this system but the results were not as good as those obtained with the dual-camera system. This is to be expected as option 3 had several additional optical components redirecting the light path, whereas in the dual-camera system, the filters were directly in front of each camera. If we were to implement the more expensive option (option 1)

Fig. 18 Screenshot of the skin detection video processed through the wavelength-switching optical box (a) without skin detection applied and (b) with skin detection.

that passed the light straight through to the camera without any reflections, we would expect the results to be better.

Another important point is that detection was poorer on parts of the subject that were moving faster. The subject was rotating in the chair for the video and moving his right hand back and forth. The right hand represented the fastest movement, as well as the poorest detection. This indicates that the frame rate that was used was likely too slow. As the hand quickly advanced, the time lag between frame captures caused it to be in different positions for the two images that were compared (1072 and 1250 filter images). By increasing the frame rate and making sure to skip as few frames as possible between frame grabs, there would be less difference in the position of the moving hand between adjacent video frames. In this case, the time required for switching between filter wavelengths caused the loss of at least one frame between differently filtered images. The ability to increase the frame rate would also be expected to improve with the more costly option 1.

7 Discussion

Skin reflectance was modeled and compared against potential environmental confusers, skin detection performance was evaluated in still images, and the concept was applied to video. Following the work of Kubelka, Meglinski, and Nunez, the skin model was created using the Fresnel and K–M equations, along with various data sets that described the concentrations and distributions of skin's many constituents. The model reflectance output provided reasonable agreement with published experimental reflectance data for both lightly and darkly pigmented skin.

The K–M approach has some inherent inaccuracies in modeling skin reflectance. In it, skin is considered to be a finite number of constant-thickness layers of homogenous optical properties, when in reality, layer thicknesses can vary and the optical properties can be inhomogeneous. The K–M theory also utilizes linear relationships between its own scattering and absorption coefficients and the scattering and absorption coefficients of the medium, when those relationships may actually be nonlinear.[47–49] Despite these inaccuracies, it was found to be appropriate and effective in the goals of this effort. Most models involve a trade-off between performance and other factors, such as processing speed and equipment cost. With enough computational power, time, and budget, high fidelity skin modeling can be accomplished. However, this effort focused on selecting filter wavelengths that could be used for achieving a real-time, reliable skin detection method that can be applied to video in the field. For these reasons, the K–M theory was appropriate.

An example of the trade-offs between performance, processing speed, and cost for skin detection methods can be seen by referring to the work of Baranoski and Chen.[34] They considered a larger spectral range (UV to IR) and applied four different wavelengths into their detection index (compared to the two used herein). Utilizing a much larger spectral range and doubling the number of optical filters may improve detection performance in this effort but would also be less practical in application. And as they pointed out, the spectrometer hardware required may still not be affordable for general use.[34] More importantly, another major consideration is the requirement of using four-wavelength filters in both the IR and visible spectrums, which would make the hardware even more complicated for video. It would either require four camera systems or a single broad-spectrum sensor and a method to rapidly switch between four filters (and capture images) at an acceptable video frame rate. The data set would also double, slowing the processing rate. A balance among performance, cost, and computational speed must be considered, especially when designing an affordable, fieldable sensor that must operate rapidly enough to keep up with typical video frame rates.

By varying the parameters in the skin model, it was readily observed that natural variations in melanosome concentration played a very large role in determining the overall reflectance in the visible and near-IR spectra. Low melanosome concentrations produced higher reflectance and vice versa. The ranges associated with blood fraction and subcutaneous reflectance exhibited moderate effects, while the influence from beta-carotene, bilirubin, and hemoglobin concentration variations were minimal. Because the goal was to be able to identify skin under various

situations, regardless of natural physiological variations, the heavy influence of melanin was avoided, driving the focus to the SWIR region.

Using the skin model, several unique skin reflectance features were identified in the SWIR region, which were compared to the reflectance of other materials that could potentially cause false detections. SWIR spectral bands were selected for investigation that represented unique skin features, differences from potential false positive materials, and that matched available commercial filter bands. These included 1072, 1250, 1550, and 1650 nm. Although the region around 1450 nm represented a unique skin reflectance feature, it was avoided due to high atmospheric absorption and low skin reflectance.

Due to its high solar irradiance, high reflectance magnitude, and relative consistency across different skin types, 1072 nm was chosen as the primary (reference) wavelength. The other wavelengths under consideration were then paired with it and used to identify ratios that would be indicative of skin, using a normalized difference index, and not representative of any potential confusers. The 1072-/1250-nm filter combination provided the best performance of the two-filter combinations, both inside under tungsten-halogen lighting, and outside under natural illumination. The other wavelength pairs (1072/1550 and 1072/1650 nm) struggled more with false detections from vegetation and shadows. Vegetation, like skin, contains a significant amount of water, which is very influential in the SWIR band. In fact, the reflectance profile of vegetation in the SWIR band is very similar to skin. The reason the 1072-/1250-nm filter combination performed better than the others with respect to vegetation is simply because the ratio between skin and vegetation reflectance at these wavelengths is greater than similar ratios for the 1072-/1550-nm and 1072-/1650-nm pairs. This can be seen in Fig. 6.

It is likely that shadows created a problem in some of the investigations because of the low light levels associated with them. As the overall level of light being reflected back diminishes, the absolute difference in reflectance measured between two different materials also reduces. Even though the reflectance ratios may not actually change, as the absolute difference in reflectance grows smaller, the ratio can become more difficult to measure and the effect of noise can cause some of them to be misinterpreted. Again, the most likely reason why the 1072-/1250-nm filter combination performed better in shadows is simply because the 1072-/1250-nm ratio difference is greater between skin and the other materials for this filter combination than it is at the others. In addition, both of these wavelengths receive relatively high solar irradiance, making for a more detectable signature. Considering the difficulties associated with shadows, one potential avenue of improvement would be to apply shadow detection algorithms to the images and treat shadows differently for skin detection. Several researchers have proposed different methods of identifying shadows in images.[19,90–94]

Another aspect to consider when evaluating skin reflectance is the variation of sampling volume with wavelength. The different constituents of skin scatter and absorb differently at different wavelengths, thereby affecting light penetration depth. And considering the layered structure of skin, it is important to know how deep light is penetrating to understand the interactions that are taking place. To engage the deeper layers, good penetration depth must be attained. Meglinski and Matcher[95] and Doronin and Meglinski[96] have discussed modeling the sampling volume for blood oxygenation measurements. In their cases, it is important for light to reach the deeper layers of skin where the vascularity resides and to understand which vascular bed is responsible for detected signals. Bashkatov et al.[97] measured the absorption and reduced scattering coefficients of human skin in the wavelength range of 400 to 2000 nm and estimated the penetration depth as a function of wavelength. Their results indicate that the absorption and reduced scattering coefficients of human skin are low in the range of the target wavelengths chosen herein (1072 and 1250 nm), and the estimated depth of penetration is high. They determined the highest penetration depth to be in the vicinity of the 1072-nm wavelength and 1250 nm fell within the second highest peak. Penetration in these ranges is higher than in the other wavelengths considered, as well anywhere in the visible range. This means that light at these wavelengths more fully interrogates skin, which may partially explain why this wavelength pair performed the best. Furthermore, Nasouri et al.[98] modeled near-IR penetration in human skin and developed a better understanding of the relative dosage received in the epidermis, dermis, and subcutaneous layers. They found that the spatial distribution of absorptivity varied considerably between the layers at different wavelengths. For example, at 1150 nm,

the epidermis and dermis contributed lower absorption, allowing the light to travel deeper, while at 1550 nm, the dermis absorbed a much larger relative percentage.

Although there were no problems with the skin model results for the goals of this effort, there may be additional ways to improve its output reflectance accuracy. This would in turn provide better indication of the ratios to look for to identify skin. The model currently assumes that all light falls normal to skin. However, in reality, this is seldom correct. This assumption is most important for the Fresnel reflection at the skin/air interface. Also, the skin/air interface was the only one that considered the index of refraction differences between adjacent layers. Although the differences in indices of refraction are less significant between the other layers of the skin, taking this into account could improve accuracy to some degree. Furthermore, skin model performance could be improved by combining experimental measurements with the modeling effort, similar to the work of Petrov et al.[76] who correlated experimentally measured spectra to Monte Carlo simulations. They measured transmission in the near-IR range for different parts of the human arm, ranging from the fingertip to the forearm, and compared them to their simulation. They were then able to present human skin in a particular color space, which was analyzed by Monte Carlo simulation in the context of human tissue functional properties, providing a potential tool for analysis of skin's physiological condition.

To contend with the false positives associated with one of the poorer performing filter combinations (1072/1550), a three-filter approach was evaluated. In this approach, an active effort was taken to identify the problematic materials for this wavelength pair (primarily vegetation) and subtract them from the skin truth image. This approach showed significant improvement over using two filters for this wavelength set. However, the drawback to this approach is the obvious one: complexity. A three-filter system is more complicated and costly than a two-filter one. And the best two-filter combination (1072/1250 nm) provided similar performance with respect to detection and false positive rejection.

The best two-filter combination (1072/1250 nm) was applied to video. Two different video configurations were constructed and tested; dual and single cameras. For the dual-camera configuration, each camera was fitted with a different optical bandpass filter and then timewise images from both cameras were processed together. Three different single-camera configurations were conceived, utilizing optical components such as bandpass filters, LC cells, and polarizers, which varied in complexity, performance, and cost. All of the options are based on multiplexing the camera frames, with alternating frames being captured with different filters. The lowest cost single-camera system was constructed to demonstrate the concept, even though it was also expected to provide the poorest performance.

Skin was adequately detected with both the dual- and single-camera configurations. However, the single-camera system did not perform as well. This is likely due to the complexity and light loss associated with the many optical components needed. This would be expected to improve with the more expensive of the single-camera configuration options proposed, which had custom parts to reduce the scattering, light loss, and complexity. Another shortcoming of the single-camera system constructed was that its performance was degraded with fast movement of the subject. This indicates that the frame rate was likely too slow, allowing the subject to move too much between frames. None the less, the concept was demonstrated and several avenues exist for future improvement.

8 Conclusion

In this effort, skin reflectance was modeled to identify unique skin features for detection, two- and three-filter skin detection methods were evaluated in still images, and the concept was applied to video using dual- and single-camera systems. Candidate wavelength bands were selected by targeting sets that represented significant differences between the modeled reflectance profiles of skin and reflectance data for various natural and synthetic materials. A three-filter approach was found to perform best with still images because it was not only used to identify skin, but it also allowed for the secondary detection and subtraction of one of the primary false positives in the SWIR band: vegetation. However, even with just two filters, the 1072-/1250-nm combination was also found to perform well.

In addition to its simplicity, the 1072-/1250-nm set is also the most appropriate for application to video for several reasons. The ratio of these two wavelengths for skin differs significantly from the same ratio of the potential false positive materials considered. The overall level of illumination is also important for video applications and these two wavelengths both offer high solar irradiance and the highest reflectances of the unique skin features identified in the SWIR band. This becomes beneficial for detection when ambient illumination levels are low. These two wavelengths also penetrate relatively deeply into skin, allowing for more complete interrogation of all of the layers. And finally, although a large difference between reflectance magnitudes is often desired for still image skin detection, this is not necessarily the case for video application because it causes the need for large differences in camera gain between the two different filters. In this regard, the smaller difference in reflectance levels between the 1072- and 1250-nm wavelengths was beneficial. Both wavelengths provide a strong signal that can be processed without significant gain changes, while providing an index that differs from other potentially confusing materials. The 1072-/1250-nm wavelength set was successfully demonstrated in video skin detection for both single- and dual-camera systems. The single-camera approach offers advantages, such as the need for only one sensor, easily matched sensor gains for both wavelengths, image coregistration, and the ability to zoom. The dual-sensor approach offers lower light loss (fewer optical components in front of sensor) and a potentially higher video frame rate.

Acknowledgments

This work has been supported by the Naval Surface Warfare Center Panama City Division Independent Applied Research Program. The views expressed herein are those of the author and do not reflect the official policy or position of the Department of the Navy, Department of Defense, or any agency of the U.S. government. Special thanks are extended to my colleagues, Rich Manley, Candace Cobb, and Carrie Delcomyn, who posed for skin detection analysis and assisted in the development and construction of the video system optical components.

References

1. R. Flewelling, "Noninvasive optical monitoring," in *The Biomedical Engineering Handbook*, J. Bronzino, Ed., pp. 1–11, IEEE Press, Boca Raton, Florida (1981).
2. J. McMurdy et al., "Photonics-based in vivo total hemoglobin monitoring and clinical relevance," *J. Biophotonics* **2**(5), 277–287 (2009).
3. E. Salomatina et al., "Optical properties of normal and cancerous human skin in the visible and near-infrared spectral range," *J. Biomed. Opt.* **11**(6), 064026 (2006).
4. L. L. Randeberg and J. Hernandez-Palacios, "Hyperspectral imaging of bruises in the SWIR spectral region," *Proc. SPIE* **8207**, 82070N (2012).
5. S. Vyas, A. Banerjee, and P. Burlina, "Estimating physiological skin parameters from hyperspectral signatures," *J. Biomed. Opt.* **18**(5), 057008 (2013).
6. D. Yudovsky and L. Pilon, "Rapid and accurate estimation of blood saturation, melanin content, and epidermis thickness from spectral diffuse reflectance," *Appl. Opt.* **49**(10), 1707–1719 (2010).
7. Q. Zhang et al., "Assessment of hemodynamic changes of pig skin in the post-burn period using a multi-spectral multi-aperture camera," Wake Forest University Technical Report, Wake Forest University Health Sciences, Winston Salem, North Carolina (2009).
8. M. A. Changizi, Q. Zhang, and S. Shimojo, "Bare skin, blood and the evolution of primate colour vision," *Biol. Lett.* **2**(2), 217–221 (2006).
9. G. A. Ramirez, "Color analysis of facial skin: detection of emotional state," in *Computer Vision and Pattern Recognition Workshops*, IEEE (2014).
10. D. Jakovels, J. Spigulis, and I. Saknite, "Multi-spectral mapping of in-vivo skin hemoglobin and melanin," *Proc. SPIE* **7715**, 77152Z (2010).
11. L. Li and C. S. Ng, "Rendering human skin using a multi-layer reflection model," *Int. J. Math. Comput. Simul.* **1**(3), 44–53 (2009).

12. E. J. Parra, "Human pigmentation variation: evolution, genetic basis, and implications for public health," *Yearbook Phys. Anthropol.* **134**, 85–105 (2007).
13. R. Zhang et al., "Determination of human skin optical properties from spectrophotometric measurements based on optimization by genetic algorithms," *J. Biomed. Opt.* **10**(2), 1–11 (2005).
14. G. B. Altshuler, R. R. Anderson, and D. Manstein, "Method and apparatus for the selective targeting of lipid-rich tissue," U.S. Patent No. 6, 605, 080 B1 (2003).
15. R. R. Anderson and J. A. Parrish, "The science of photomedicine," in *Optical Properties of Human Skin*, J. D. Regan et al., Ed., Plenum Press, New York (1982).
16. L. O. Svaasand et al., "Tissue parameters determining the visual appearance of normal skin and port-wine stains," *Lasers Med. Sci.* **10**, 55–65 (1995).
17. H. Chang, "Multispectral imaging for face recognition over varying illumination," PhD Dissertation, The University of Tennessee (2008).
18. M. T. Eismann, "Strategies for hyperspectral target detection in complex background environments," in *IEEE Aerospace Conf.*, Big Sky, Montana (2006).
19. S. G. Kong et al., "Adaptive fusion of visual and thermal IR images for illumination-invariant face recognition," *Int. J. Comput. Vision* **71**(2), 215–233 (2007).
20. B. Martinkauppi, "Face colour under varying illumination—analysis and applications," PhD Dissertation, University of Oulu (2002).
21. S. J. Schmugge et al., "Objective evaluation of approaches of skin detection using ROC analysis," *Comput. Vision Image Understanding* **108**, 41–51 (2007).
22. M. Storring, "Computer vision and human skin colour," PhD Dissertation, Aalborg University (2004).
23. D. Saxe and R. Foulds, "Toward robust skin identification in video images," in *Proc. 2nd Int. Conf. on Automatic Face and Gesture Recognition*, pp. 379–384 (1996).
24. R. L. Hsu, M. Abdel-Mottaleb, and A. K. Jain, "Face detection in color images," *IEEE Trans. Pattern Anal. Mach. Intell.* **24**(5), 696–706 (2002).
25. M. J. Jones and J. M. Rehg, "Statistical color models with application to skin detection," *Int. J. Comput. Vision* **46**(1), 81–96 (2002).
26. M. H. Yang and N. Ahuja, "Detecting human faces in color images," in *Proc. 1998 Int. Conf. on Image Processing*, pp. 127–130 (1998).
27. K.-M. Cho, J.-H. Jang, and K.-S. Hong, "Adaptive skin-color filter," *Pattern Recognit.* **34**(5), 1067–1073 (2001).
28. Y. Raja, S. J. McKenna, and G. Gong, "Tracking and segmenting people in varying lighting conditions using colour," in *Proc. IEEE 3rd Int. Conf. on Automatic Face and Gesture Recognition*, pp. 228–233 (1998).
29. T. W. Yoo and I. S. Oh, "A fast algorithm for tracking human faces based on chromaticity histograms," *Pattern Recognit. Lett.* **20**(10), 967–978 (1999).
30. E. Angelopoulou, "Understanding the color of human skin," *Proc. SPIE* **4299**, 243–251 (2001).
31. J. Zeng et al., "Human detection in non-urban environment using infrared images," in *6th Int. Conf. on Information Communications & Signal Processing*, pp. 1–4 (2007).
32. L. M. Son, D. Chai, and A. Bouzerdoum, "A universal and robust human skin color model using neural networks," in *Proc. IJCNN'01 Int. Joint Conf. on Neural Networks*, pp. 2844–2849 (2001).
33. A. S. Nunez, "A physical model of human skin and its application for search and rescue," PhD Dissertation, Air Force Institute of Technology (2009).
34. G. V. G. Baranoski and T. F. Chen, "Multispectral index for the remote detection of human skin signatures," *Opt. Eng.* **54**(7), 070502 (2015).
35. P. Kubelka, F. Munk, and F. Zeits, "Ein beitrag zur optik der farbanstriche," *Tech. Phys.* **12**, 593–601 (1931).
36. P. Kubelka, "New contributions to the optics of intensely light-scattering materials," *J. Opt. Soc. Am.* **38**(5), 448–457 (1948).
37. P. Kubelka, "New contributions to the optics of intensely light-scattering materials. Part II: nonhomogeneous layers," *J. Opt. Soc. Am.* **44**(4), 330 (1954).
38. J. B. Dawson et al., "A theoretical and experimental study of light absorption and scattering by in vivo skin," *Phys. Med. Biol.* **25**(4), 695–709 (1980).

39. I. V. Meglinski and S. J. Matcher, "Quantitative assessment of skin layers absorption and skin reflectance spectra simulation in the visible and near-infrared spectral regions," *Physiol. Meas.* **23**, 741–753 (2002).
40. H. Du et al., "PhotochemCAD: a computer-aided design and research tool in photochemistry," *Photochem. Photobiol.* **68**, 141–142 (1998).
41. S. Prahl, "Tabulated molar extinction coefficient for hemoglobin in water," Wellman Laboratories, Harvard Medical School, Boston (2015).
42. R. M. Pope and E. S. Fry, "Absorption spectrum (380–700 nm) of pure water. II. Integrating cavity measurements," *Appl. Opt.* **36**(33), 8710–8723 (1997).
43. K. F. Palmer and D. Williams, "Optical properties of water in the near infrared," *J. Opt. Soc. Am.* **64**, 1107–1110 (1974).
44. R. L. P. van Veen et al., "Determination of VIS- NIR absorption coefficients of mammalian fat, with time and spatially resolved diffuse reflectance and transmission spectroscopy," in *OSA Annual BIOMED Topical Meeting* (2004).
45. T. Sarna and H. M. Swartz, "The physical properties of melanins," in *The Pigmentary System*, J. J. Nordlund et al., Ed., Oxford University Press, New York (1988).
46. A. J. Thody et al., "Pheomelanin as well as eumelanin is present in human epidermis," *J. Invest. Dermatol.* **97**(2), 340–344 (1991).
47. L. Yang and B. Kruse, "Revised Kubelka–Munk theory. I. Theory and application," *J. Opt. Soc. Am. A* **21**(10), 1933–1941 (2004).
48. L. Yang, B. Kruse, and S. J. Miklavcic, "Revised Kubelka–Munk theory. II. Unified framework for homogeneous and inhomogeneous optical media," *J. Opt. Soc. Am. A* **21**(10), 1942–1952 (2004).
49. L. Yang and S. J. Miklavcic, "Revised Kubelka–Munk theory. III. A general theory of light propagation in scattering and absorptive media," *J. Opt. Soc. Am. A* **22**(9), 1866–1873 (2005).
50. J. Fore-Pfliger, "The epidermal skin barrier: implications for the wound care practitioner, Part I," *Advances in Skin and Wound Care*, 417–425 (2004).
51. D. Koruga et al., "Epidermal layers characterisation by opto-magnetic spectroscopy based on digital image of skin," *Acta Phys. Pol. A* **121**(3), 606–610) (2012).
52. G. Chapman, *The Body Fluids And Their Functions*, Edward Arnold, London (1980).
53. K. S. Stenn, *The Skin Cell and Tissue Biology*, L. Weiss, Ed., pp. 541–572, Urban and Schwarzenberg, Baltimore, Maryland (1988).
54. G. F. Odland, *Structure of the Skin, Physiology, Biochemistry, and Molecular Biology of the Skin*, L. A. Goldsmith, Ed., Vol. **1**, pp. 3–62, Oxford University Press, Oxford (1991).
55. K. A. Holdbrook, *Structure and Functions of the Developing Human Skin, Physiology, Biochemisty, and Molecular Biology of the Skin*, L. A. Goldsmith, Ed., Vol. **1**, pp. 63–112, Oxford University Press, Oxford (1991).
56. E. M. Renkin, C. C. Michel, and S. R. Geiger, "Handbook of physiology. Section 2: the cardiovascular system," in *Microcirculation Part 1*, Vol. **IV**, American Physiological Society, Bethesda, Maryland (1984).
57. T. J. Ryan, *Cutaneous Circulation, Physiology, Biochemistry, and Molecular Biology of the Skin*, L. A. Goldsmith, Ed., Vol. **2**, pp. 1019–1084, Oxford University Press, Oxford (1991).
58. S. L. Jacques, *Origins of Tissue Optical Properties in the UVA, Visible and NIR Regions, Advances in Optical Imaging and Photon Migration*, R. R. Alfano and J. G. Fujimoto, Eds., Vol. **2**, pp. 364–370, OSA, Washington, DC (1996).
59. R. O. Potts, "Stratum corneum hydration: experimental techniques and interpretations of results," *J. Soc. Cosmet. Chem.* **37**, 9–33 (1985).
60. A. Karishnaswamy, "BioSpec: a biophysically-based spectral model of light interaction with human skin," MS Thesis, University of Waterloo (2005).
61. I. S. Saidi, S. L. Jacques, and F. K. Tittel, "Mie and Rayleigh modeling of visible-light scattering in neonatal skin," *Appl. Opt.* **34**(31), 7410–7418 (1995).
62. C. R. Lovell, "Type I and III collagen content and fibre distribution in normal human skin during ageing," *Br. J. Dermatol.* **117**, 419–428 (1987).
63. S. L. Jacques, "Skin optics," Oregon Medical Laser Center News, 1998, http://omlc.ogi.edu/news/jan98/skinoptics.html (15 January 2015).

64. S. L. Jacques, R. D. Glickman, and J. A. Schwartz, "Internal absorption coefficient and threshold for pulsed laser disruption of melanosomes isolated from retinal pigment epithelium," *Proc. SPIE* **2681**, 468 (1996).
65. R. Lee et al., "The detection of carotenoid pigments in human skin," *J. Invest. Dermatol.* **64**, 175–177 (1975).
66. A. Yaroslavsky et al., "Optics of blood," in *Handbook of Optical Biomedical Diagnostics*, V. Tuchin, Ed., pp. 169–216, SPIE Press, Bellingham, Washington (2002).
67. B. Rolisky et al., "Total bilirubin measurement by photometry on a blood gas analyser: potential for use in neonatal testing at point of care," *Clin. Chem.* **47**(10), 1845–1847 (2001).
68. S. L. Schutz, *Oxygen Saturation Monitoring by Pulse Oximetry, AACN Procedure Manual for Critical Care*, 4th ed., D. J. Lynn-McHale, K.K. Carlson, and W. B. Saunders, Eds., pp. 76–82 (2001).
69. P. Van Beest et al., "Clinical review: use of venous oxygen saturations as a goal—a yet unfinished puzzle," *Crit. Care* **15**(232), 1–9 (2011).
70. G. Kandel and A. Aberman, "Mixed venous oxygen saturation. Its role in the assessment of the critically ill patient," *Arch. Intern. Med.* **143**(7), 1400–1402 (1983).
71. L. D. Nelson, "Continuous venous oximetry in surgical patients," *Ann. Surg.* **203**(3), 329–333 (1986).
72. A. Keys, "The oxygen saturation of the venous blood in normal human subjects," *Am. J. Physiol.* **124**, 13–21 (1938).
73. E. Hecht, *Optics*, Addison-Wesley, Reading, Massachusetts (2002).
74. M. Gurevic, "Ubereine rationelle klassifikation der lichtenstreuenden medien," *Phys. Z* **31**, 753 (1930).
75. H. Zocher, *Kolloidchemisches Taschenbuck*, 3rd ed., p. 83, Akademische Verlagsgesellschaft Geest & Portig KG, Leipzig (1948).
76. G. I. Petrov et al., "Human tissue color as viewed in high dynamic range optical spectral transmission measurements," *Biomed. Opt. Express* **3**(9), 2154–2161 (2012).
77. L. F. A. Douven and G. W. Lucassen, "Retrieval of optical properties of skin from measurement and modelling the diffuse reflectance," *Proc. SPIE* **3914**, 312 (2000).
78. T. F. Chen et al., "Hyperspectral modeling of skin appearance," *ACM Trans. Graph.* **34**(3), 1–14 (2015).
79. C. C. Cooksey, B. K. Tsai, and D. W. Allen, "Spectral reflectance variability of skin and attributing factors," *Proc. SPIE* **9461**, 94611M (2015).
80. J. A. Jacquez et al., "The spectral reflectance of human skin in the region 235–700 mu," *J. Appl. Physiol.* **8**(2), 212–214 (1955).
81. J. A. Jacquez et al., "The spectral reflectance of human skin in the region 0.7–2.6 mu," *J. Appl. Physiol.* **8**(3), 297–299 (1955).
82. C. C. Cooksey, B. K. Tsai, and D. W. Allen, "A collection and statistical analysis of skin reflectance signatures for inherent variability over the 250 nm to 2500 nm spectral range," *Proc. SPIE* **9082**, 908206 (2014).
83. A. M. Baldridge et al., "The ASTER spectral library version 2.0," *Remote Sens. Environ.* **113**, 711–715 (2009).
84. N. A. Streck, D. Rundquist, and J. Connot, "Spectral signature of selected soils," *Rev. Bras. Agrometeorologia* **11**(1), 181–184 (2003).
85. R. N. Clark et al., "USGS digital spectral library 06, digital data series 231," 2013, Denver, Colorado, http://speclab.cr.usgs.gov/spectral.lib06 (15 January 2015).
86. "Reference solar spectral irradiance: ASTM G-173, derived from SMARTS (simple model of the atmospheric radiative transfer of sunshine) v. 2.9.2, NREL (National Renewable Energy Laboratory)," Golden, Colorado, http://rredc.nrel.gov/solar/spectra/am1.5/astmg173/astmg173.html (26 January 2015).
87. G. M. Smith and E. J. Milton, "The use of the empirical line method to calibrate remotely sensed data to reflectance," *Int. J. Remote Sens.* **20**(13), 2653–2662 (2010).
88. J. R. G. Townshend and C. O. Justice, "Analysis of the dynamics of African vegetation using the normalized difference vegetation index," *Int. J. Remote Sens.* **7**(11), 1435–1445 (1986).

89. A. J. Elmore et al., "Quantifying vegetation change in semiarid environments: precision and accuracy of spectral mixture analysis and the normalized difference vegetation index," *Remote Sens. Environ.* **73**(1), 87–102 (2000).
90. J. A. Marchant and C. M. Onyango, "Shadow-invariant classification for scenes illuminated by daylight," *J. Opt. Soc. Am. A* **17**(11), 1952–1961 (2000).
91. D. Rufenacht, C. Fredembach, and S. Susstrunk, "Automatic and accurate shadow detection using near-infrared information," *IEEE Trans. Pattern Anal. Mach. Intell.* **36**(8), 1672–1678 (2014).
92. B. Khanal and D. Sidibe, "Efficient skin detection under severe illumination changes and shadows," in *4th Int. Conf. Intelligent Robotics and Applications (ICIRA 2011)*, Aachen, Germany, Vol. 7102, pp. 609–18 (2011).
93. C. O. Conaire, N. E. O'Connor, and A. F. Smeaton, "Detector adaptation by maximising agreement between independent data sources, computer vision and pattern recognition," in *IEEE Conf. on (CVPR'07)*, Minneapolis, Minnesota, pp. 1–6 (2007).
94. Y. S. Heo, K. M. Lee, and S. U. Lee, "Mutual information-based stereo matching combined with SIFT descriptor in log-chromaticity color space, computer vision and pattern recognition," in *IEEE Conf. on (CVPR 2009)*, Miami, Florida, pp. 445–452 (2009).
95. I. V. Meglinski and S. J. Matcher, "Modelling the sampling volume for skin blood oxygenation measurements," *Med. Biol. Eng. Comput.* **39**(1), 44–50 (2001).
96. A. Doronin and I. Meglinski, "Online object oriented Monte Carlo computational tool for the needs of biomedial optics," *Biomed. Opt. Express* **2**(9), 2461 (2011).
97. A. N. Bashkatov et al., "Optical properties of human skin, subcutaneous and mucous tissues in the wavelength range from 400 to 2000 nm," *J. Phys. D: Appl. Phys.* **38**, 2543–2555 (2005).
98. B. Nasouri, T. E. Murphy, and H. Berberoglu, "Near infrared laser penetration and absorption in human skin," *Proc. SPIE* **8932**, 893207 (2014).

Tye Langston holds degrees in mechanical and ocean engineering, as well as a professional engineer license. Currently, he works with the Intelligent Sensing and Irregular Warfare Group at the Naval Surface Warfare Center in Panama City, Florida. Previously, he worked in the submarine engineering division of Newport News Shipbuilding. His research interests are varied, with previous work including explosive and human sensors, composite materials, and body armor.